AGU ADVANCING EARTH AND SPACE SCIENCES

Geophysical Research Letters

RESEARCH LETTER
10.1029/2024GL111937

Biogeochemical-Argo Floats Reveal Seasonality of the Biological Carbon Pump Influenced by the Lofoten Basin Eddy

D. Koestner[1], S. Clayton[2], P. Lerner[3], A. E. Jones-Kellett[4,5], and S. L. Walker[6]

[1]Department of Physics and Technology, University of Bergen, Bergen, Norway, [2]Ocean BioGeosciences, National Oceanography Centre, Southampton, UK, [3]Department of Applied Physics and Applied Mathematics, Columbia University, New York, NY, USA, [4]Department of Earth, Atmospheric and Planetary Sciences, Massachusetts Institute of Technology, Cambridge, MA, USA, [5]Biology Department, Woods Hole Oceanographic Institution, Woods Hole, MA, USA, [6]School of Oceanography, University of Washington, Seattle, WA, USA

Key Points:

- Epipelagic waters influenced by the Lofoten Basin Eddy (LBE) show increased oxygen use and lower proportions of large particles than nearby water
- The twilight zone influenced by the LBE has lower concentrations of particulate organic carbon (POC) than surrounding waters
- The LBE has distinct biogeochemical signatures with less effective organic carbon export and complex seasonal variations

Supporting Information:

Supporting Information may be found in the online version of this article.

Correspondence to:

D. Koestner,
daniel.koestner.optics@gmail.com

Citation:

Koestner, D., Clayton, S., Lerner, P., Jones-Kellett, A. E., & Walker, S. L. (2025). Biogeochemical-Argo floats reveal seasonality of the biological carbon pump influenced by the Lofoten Basin Eddy. *Geophysical Research Letters*, *52*, e2024GL111937. https://doi.org/10.1029/2024GL111937

Received 12 AUG 2024
Accepted 12 MAY 2025

Author Contributions:

Conceptualization: D. Koestner
Data curation: D. Koestner, A. E. Jones-Kellett
Formal analysis: D. Koestner, S. Clayton, P. Lerner
Investigation: D. Koestner, S. Clayton, P. Lerner, A. E. Jones-Kellett, S. L. Walker
Methodology: D. Koestner, S. Clayton, P. Lerner, A. E. Jones-Kellett, S. L. Walker
Software: D. Koestner, P. Lerner
Visualization: D. Koestner, S. Clayton, P. Lerner
Writing – original draft: D. Koestner

Abstract The Lofoten Basin Eddy (LBE) is a persistent topographically constrained anticyclonic eddy in the Norwegian Sea. Considering its local, dynamically distinct state, we test the hypothesis that the LBE has unique biogeochemical signatures. Using satellite observations and a 12-year Biogeochemical-Argo float record, we constructed a climatological view of the annual biogeochemical cycle within and surrounding the LBE. The biological carbon pump influenced by the LBE was less effective than surrounding waters, particularly during late spring. Particulate organic carbon export out of the productive zone was hindered during summer and likely associated with enhanced respiration and slower particle sinking speeds. Enhanced export into the twilight zone was also observed and consistent with shoaling of deep mixed layers in early spring, production of large particles in late summer, and subduction in late autumn; however, these mechanisms appear to be accompanied by enhanced remineralization within the LBE influence zone, highlighting the biogeochemical complexity of eddies.

Plain Language Summary Anticyclonic eddies alter the vertical water column by deepening density layers and often locally increasing temperature. These features are present across the global ocean and affect marine organismal growth and the rates of carbon export to the deep ocean. Due to the seafloor terrain in the Norwegian Sea, an anticyclone persists year-round, known as the Lofoten Basin Eddy (LBE). Here we used data from a suite of robotic drifters that have collected nearly 12 years of continuous observations of the vertical water column, including temperature, oxygen, and proxies for particulate organic carbon. We found evidence within the LBE influence zone for increased heterotrophic feeding and slower particle sinking speeds, which reduces the effectiveness of organic carbon transport to the deep ocean. The persistent nature of the LBE, coupled with its influence on heterotrophic activity and particle sinking rates, suggests that it plays an important role in the ocean-atmosphere carbon system, modulating regional ocean carbon sequestration dynamics in an Arctic marginal sea.

1. Introduction

Mesoscale eddies with characteristic scales O(10–100 km) are ubiquitous features in the global ocean and play an important role in energy transfer and setting the distribution of biogeochemical properties (Lévy et al., 2024; McGillicuddy, 2016). However, the net impacts of mesoscale eddies on ocean biogeochemistry and carbon export are difficult to quantify observationally due to their short lifespans (~months) and evolving characteristics (Resplandy et al., 2019). Previous investigations of mesoscale eddies have showcased enhanced carbon export driven by physical mechanisms (e.g., Lacour et al., 2023; Omand et al., 2015; Stukel et al., 2017), but often capture the dynamics for only a portion of the eddy lifespan. In the current study, we seek to understand the evolution of organic carbon in the persistent anticyclonic Lofoten Basin Eddy (LBE) with a monthly composite view of its biological carbon pump.

The LBE, located in the Lofoten Basin of the Norwegian Sea (Søiland & Rossby, 2013), was identified as early as 1900 with recordings of localized thermocline deepening (Helland-Hansen & Nansen, 1909). Its permanence is due to the bathymetric depression of the Lofoten Basin, eddy merging from the Norwegian Atlantic Current, and deep winter mixing (Bosse et al., 2019; Köhl, 2007; Rossby et al., 2009; Søiland et al., 2016). As the largest

Writing – review & editing: D. Koestner, S. Clayton, P. Lerner, A. E. Jones-Kellett, S. L. Walker

standing eddy in the Nordic Seas, it likely influences the climate of Scandinavia and sea ice cover in the Barents Sea (Isachsen et al., 2012).

Here, we leverage the 12-year presence of Biogeochemical (BGC)-Argo floats in the Norwegian Sea to study biogeochemical processes influenced by the LBE. We track average monthly changes in the mass concentration of particulate organic carbon (POC), which serves as the foundation for marine food webs and is comprised of phytoplankton, heterotrophic organisms, and non-living organic detritus. We examine vertical distributions of small and large POC stocks to discern variations in net organic carbon production and export influenced by the LBE. These processes are core to understanding the strength and efficiency of the regional biological carbon pump governing the fate of organic carbon in the ocean, some of which serves as long-term storage of atmospheric CO_2 in the deep ocean (Boyd & Trull, 2007; Volk & Hoffert, 1985). Comprehending these net mesoscale production and export processes is crucial to predicting future atmospheric CO_2 levels (Honjo et al., 2014).

2. Materials and Methods

2.1. Biogeochemical-Argo Float and Eddy Co-Location

We identified the LBE from January 2010 to February 2022 from satellite altimetry using the AVISO META3.2 DT allsat eddy atlas (Text S1 in Supporting Information S1; Mason et al., 2014; Pegliasco, Delepoulle, et al., 2022). Eddy contours were scaled by a factor of 1.5 (as in Wang et al., 2023) to determine the Lofoten Basin Eddy influence Zone (LBEZ) which contains the eddy core and influence zone. The average effective radius of the LBEZ was 85 km (Figure S1 in Supporting Information S1). We utilized 1521 profiles from 22 BGC-Argo floats located in the LBEZ and surrounding waters (67.5–72.5°N, 7°W–15°E; Figure 1a). The floats resolve the particulate backscattering coefficient (b_{bp}), chlorophyll-a concentration (Chla), dissolved oxygen concentration (DO), temperature (T), and salinity, with some also estimating photosynthetically active radiation and nitrate concentration. The BGC-Argo profiles co-located with the LBEZ using a 2-day tolerance window were considered *inside* LBEZ; the remaining profiles in the bounding box were defined as *outside* LBEZ.

2.2. Biogeochemical Data

A brief overview of essential data processing follows, with additional details in Text S2 in Supporting Information S1. b_{bp} and Chla were partitioned into small and large particle pools as described in Briggs et al. (2020), where large particles were assumed > ~100–200 μm in diameter. Small and large particle data were treated as independent variables (denoted with subscripts s and l, respectively) to calculate POC with a multivariable approach based on b_{bp} and Chla (Koestner et al., 2024).

Apparent oxygen utilization (AOU) was defined as the difference in observed DO from the concentration at 100% saturation (DO_{sat}); DO_{sat} depends on temperature, salinity, and pressure. AOU is commonly used to estimate the amount of respiration that has occurred in a parcel of water since ventilation, although it can be sensitive to other sources of oxygen undersaturation such as mixing of oxygen-depleted deep waters and processes inhibiting air-sea gas transfer (Ito et al., 2004). Nonetheless, AOU is a useful proxy for tracking metabolic differences between nearby water parcels.

All variables were averaged into 5-m bins after calculation of surface mixed layer and euphotic zone depths (MLD and EZD), and 20-m bins were used below the epipelagic zone (200–1,000 m). The productive zone (PZ) was defined as above the depth (PZD) corresponding to the deepest of the surface MLD (based on potential density) and EZD (typically based on Chla; see Text S2 in Supporting Information S1), indicative of the portion of the water column recently or actively supporting primary production. The twilight zone (TZ) refers to the remainder of the water column (PZD–1,000 m) and was further partitioned into upper and lower portions.

Monthly average profiles for each variable were finally derived as the arithmetic mean of data within each depth-bin inside or outside the LBEZ, and uncertainties were assessed with 95% confidence intervals (Student's t-test). A depth-integrated POC (iPOC) approach was adopted following Dall'Olmo and Mork (2014). POC was integrated within the PZ and TZ on a profile-by-profile basis for small and large particle pools to determine monthly mean iPOC. These iPOC values were used to determine mean monthly net fluxes describing *total* ($iPOC_s$ + $iPOC_l$) accumulation (e.g., primary production, advection, or sinking into the zone) or losses (e.g., grazing, remineralization, or sinking beneath the zone) within each zone. For example, flux within the TZ,

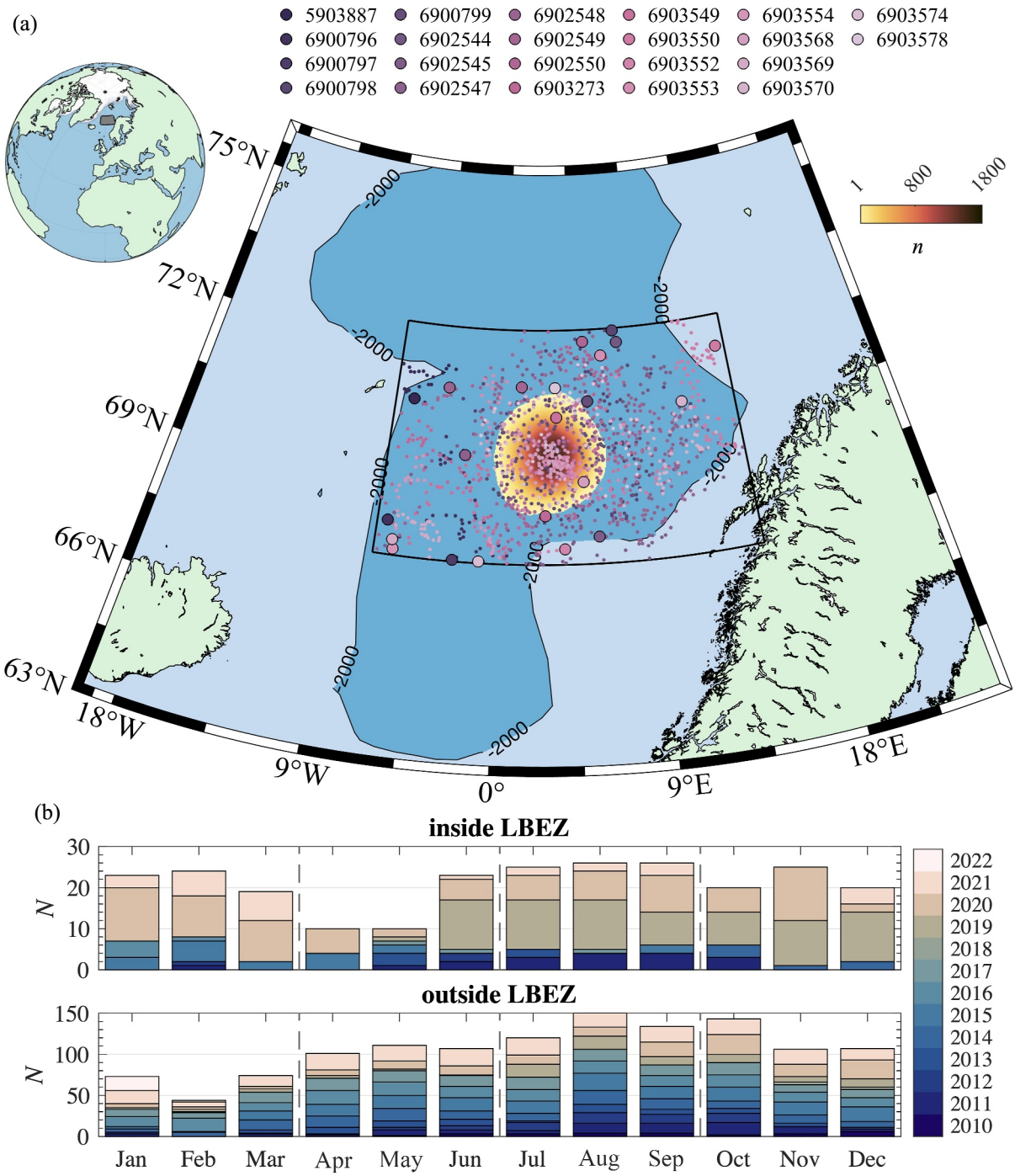

Figure 1. (a) Map of study region including BGC-Argo float locations 2010–2022. The heatmap shows the relative extent of the LBEZ during the timeseries where *n* indicates number of occurrences. WMO IDs for the 22 floats are shown. Small and large circles represent all and last profiling locations, respectively. See also Movie S1. (b) Stacked bar graphs showing number of profiles (*N*) for each month and year. Vertical dashed lines display seasonal boundaries.

$E^{TZ} = \frac{\Delta iPOC^{TZ}(t)}{\Delta t}$, where $iPOC^{TZ}(t) = \int_{PZD}^{1000\ m} POC(z,t)\,dz$ and was calculated for monthly timesteps. Fluxes were similarly computed for the PZ and lower-TZ (PZD^{+x}–1,000 m), and for $iPOC_s$ and $iPOC_l$. Transfer efficiency (TE) is defined as $TE^x = \frac{E^{PZD+x\ -\ 1000\ m}}{E^{TZ}}$ and indicative of the biological carbon pump's efficiency to transport material *x* m below the PZ. Although many depth horizons can be considered (Buesseler et al., 2020), we use $x = 200$ and 500 m to showcase efficiency to intermediate and deeper depths. A low TE suggests significant losses

in the upper x m of the TZ, while a high value indicates highly effective transport of material within this upper-TZ (see Text S5 in Supporting Information S1 for further discussion of TE uncertainty and interpretation).

An additional metric was computed describing the depth associated with 50% of the total water-column iPOC (i.e., z^{50}). For example, $z_s^{50} = 100$ m indicates that 50% of all POC_s is contained within the upper 100 m and is a useful parameter for intercomparing POC profiles.

3. Results

3.1. Depth Profiles

Vertical profiles of T and POC_s are shown in Figure 2 and differences between mean monthly profiles of T, POC_s, POC_l, and AOU inside and outside the LBEZ are shown in Figure 3. Within the LBEZ, T near the surface was ~5–6°C in winter and autumn, with maximum values ~8°C in late summer. LBEZ temperature profiles at intermediate depths (~200–600 m) were uniform throughout the year, sustaining temperatures ~5°C with small variability (mean coefficient of variation = 7%). This feature of the LBEZ is indicative of successful anticyclonic eddy identification (Raj et al., 2016), and diagnostic of particularly deep mixed layers ranging ~200–800 m for December through April after which a shallower surface mixed layer of warmer water forms. The LBEZ exhibits the greatest variability in temperature (~0–5°C) deeper than ~800 m for all months, whereas the temperature at those depths were consistently ~0°C outside the LBEZ. Surface waters in summer and autumn were often cooler inside the LBEZ, although temperatures were rarely >1°C cooler below the productive zone. The LBEZ subsurface was consistently warmer than surrounding waters, especially below 400 m where differences were >0.5°C year-round and as much as 4°C warmer below 600 m. MLDs inside and outside the LBEZ were similar June–November (mean difference = 8%) and, on average, 240 m deeper December–May.

The seasonal evolution of POC_s was similar inside and outside the LBEZ, with some notable exceptions. During winter months, when light is most limiting to primary production, there was a more uniform water column of POC_s with values typically <10 mg m^{-3} both inside and outside the LBEZ. Early indications of elevated primary production appeared in March. As light availability increased, POC_s in the surface increased inside and outside the LBEZ, with maximum values >100 mg m^{-3} first occurring around June. A typical profile with rapidly decreasing POC_s with depth in the upper 200 m is visible for most of the productive months (May–October). POC_s was on average 11 (range 0–17) mg m^{-3} *lower* in the upper 50 m of the LBEZ during April and May, but 15 (range 1–47) mg m^{-3} *higher* June and July compared to its surroundings (Figure 3f). Average EZDs were 30–116 m and similar both inside and outside the LBEZ (mean difference <3%; Figure S4 in Supporting Information S1). During late autumn and winter, POC_s profiles exhibited the most pronounced differences inside versus outside the LBEZ. A small increase in POC_s was observed inside the LBEZ at ~200–800 m, manifesting as a bulge in the profiles visible most clearly in December, but also in January and February (Figures 2i and 2l). A weaker, but similar bulge is also seen in January and February outside LBEZ (Figure 2m). Except for June, POC_s was consistently lower inside versus outside the LBEZ below 900 m (Figure 3f).

Both inside and outside the LBEZ show a typical pattern of lower AOU in the upper 50 m where the bulk of primary production occurs (Figures 3d, 3e, 3j, and 3k). At these shallow depths, AOU was negative when primary production was highest May–August. There may have been higher primary production inside the LBEZ, as AOU was ~3 μM more negative and POC_s was ~19 mg m^{-3} higher on average in the upper 15 m May–July (Figures 3f and 3l). There was on average 15% higher AOU within the upper 200 m of the LBEZ compared with its surroundings; a depth-zone that is likely ventilated due to winter mixing inside and outside LBEZ. There was consistently lower AOU inside the LBEZ below 400 m, although it is difficult to separate the effects of recent ventilation and respiration because of deep winter MLDs inside the LBEZ.

3.2. Depth-Integrated POC

$iPOC_s^{PZ}$ was 0.9–6.6 g m^{-2}, peaking in June inside and outside the LBEZ (yellow bars in Figure 4a). In contrast, $iPOC_s^{TZ}$ peaked at 6.4 g m^{-2} in September and 7.5 g m^{-2} in July with minima 0.6 g m^{-2} in April and 2.3 g m^{-2} in March for inside and outside the LBEZ, respectively. Except for June, December, and January, total water-column $iPOC_s$ was on average 20% higher *outside* the LBEZ, while $iPOC_s^{PZ}$ was 6%–22% higher *inside* LBEZ June–November. $iPOC_s^{PZ}$ was the most statistically different inside the LBEZ during winter (mostly relating to MLD differences) and June–August (Figure S6 in Supporting Information S1). In terms of vertical distribution,

10.1029/2024GL111937

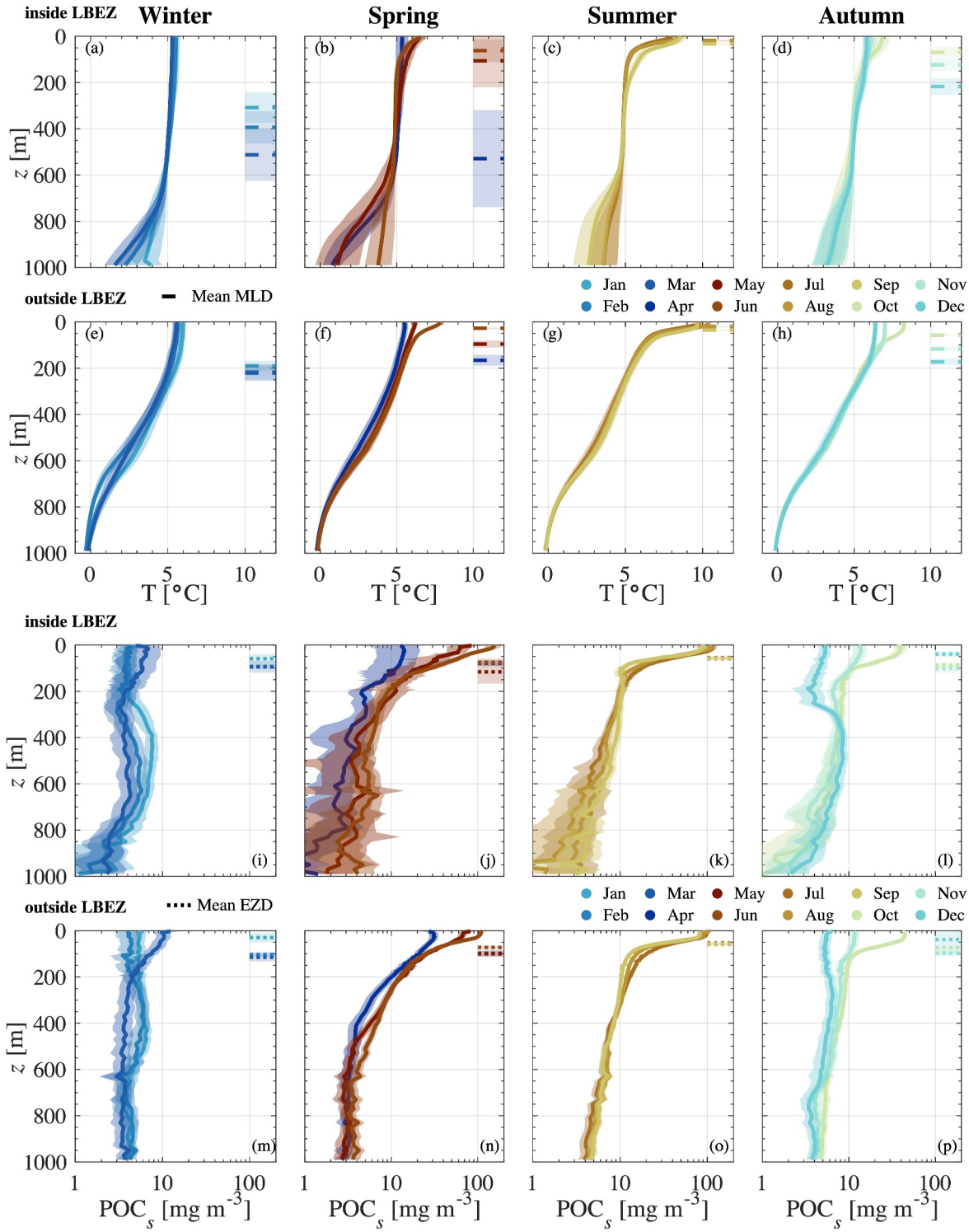

Figure 2. Monthly vertical profiles of (a–h) temperature and (i–p) POC_s inside and outside of the LBEZ. Solid lines indicate mean (horizontal dashed for MLD, dotted for EZD), while shaded regions indicate 95% confidence interval. Note that POC_s <1 mg m^{-3} is unlikely to be resolved by the optical methods employed (Koestner et al., 2024), and LBEZ POC_s profiles exhibited more statistical noise than outside-LBEZ owing to fewer available measurements (Figure 1b).

10.1029/2024GL111937

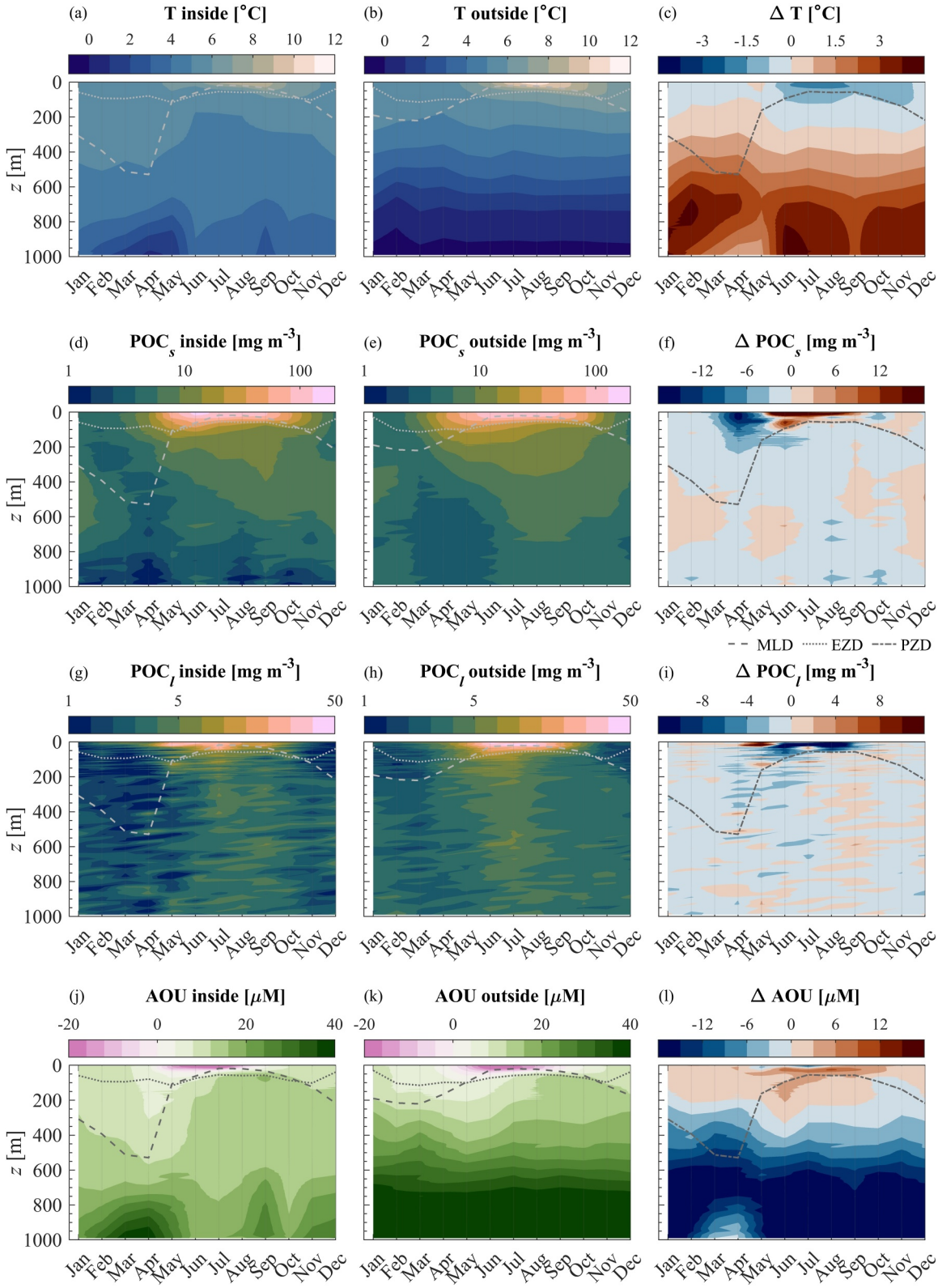

Figure 3. Mean monthly profiles (a, d, g, j) inside and (b, e, h, k) outside the LBEZ, and (c, f, i, l) the difference determined as inside minus outside LBEZ. Dashed, dotted, and dash-dotted lines represent mean MLD, EZD, and PZD, respectively. Panels (c, f, i, l) display inside-LBEZ PZDs. Data shown were interpolated using MATLAB's bilinear interpolation shading.

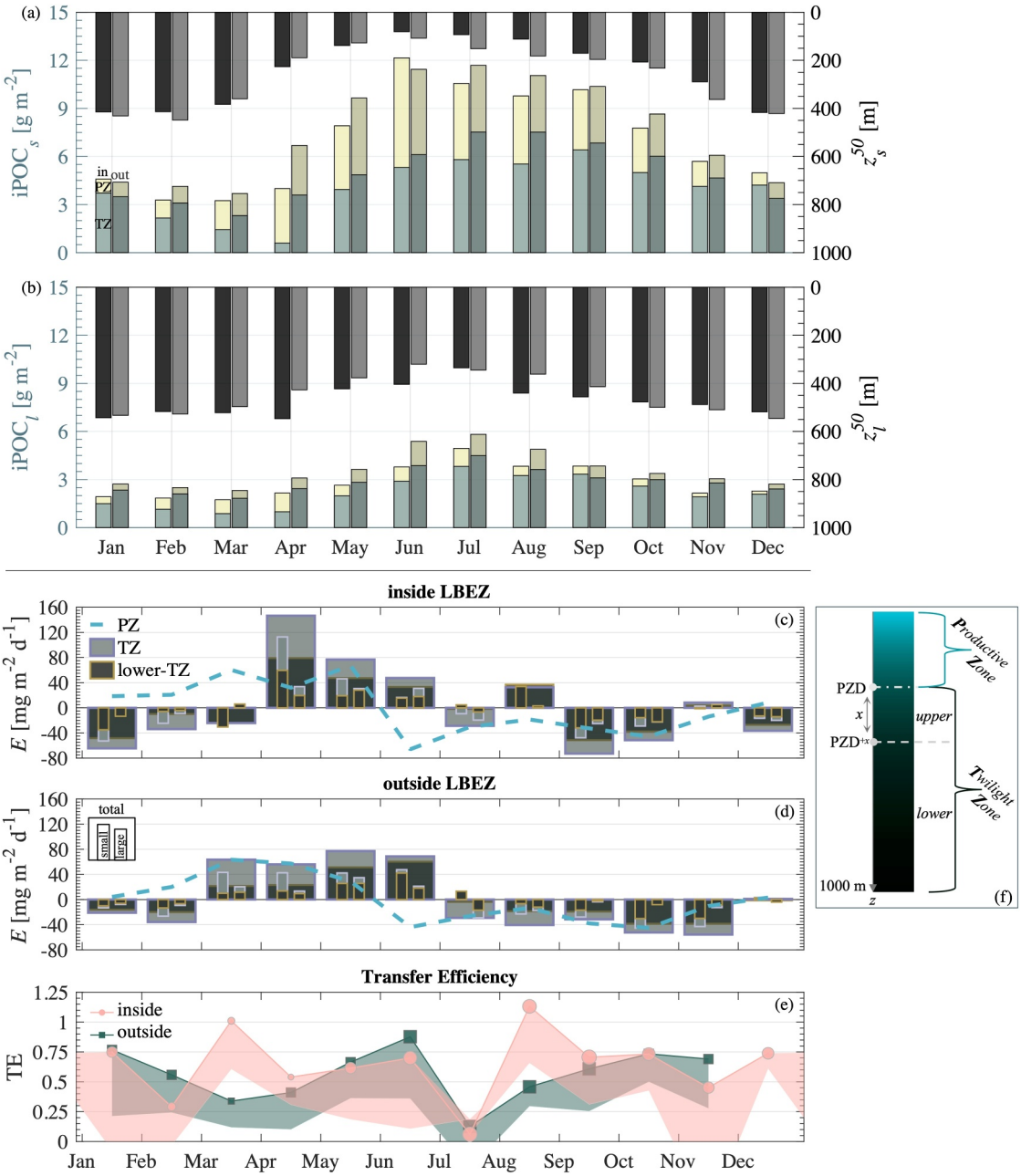

Figure 4. Summary of depth-integrated particulate organic carbon (POC) in panel (a) small and (b) large particle pools. Each bar represents monthly mean total water-column integrated POC, with color indicating quantity in productive and twilight zones. Each set of bars refers to inside (left) and outside (right) LBEZ. Additional black (inside) and gray (outside) bars extending from the top represent z^{50} (c, d) Net mean monthly fluxes for iPOC in the PZ and TZ. Fluxes in the TZ are partitioned between upper and lower with $x = 200$ m. (e) Transfer efficiencies for *total* iPOC, where upper line and marker represent TE^{200} with size of marker proportional to $iPOC^{TZ}$, and bottom of shaded region represents TE^{500}. TEs for December outside-LBEZ are not shown due to uncertainties (Text S5 in Supporting Information S1). (f) Schematic illustrating water-column partitioning.

the majority of $iPOC_s$ was below 400 m in less productive months, while 50% of $iPOC_s$ was shallower than 200 m during more productive months ($z^{50}{}_s$; Figure 4a). Except for March–May, the outside-LBEZ $z^{50}{}_s$ was 5–70 m deeper, suggesting vertical POC_s profiles were skewed deeper outside the LBEZ compared with inside.

$iPOC_l$ exhibited similar seasonal patterns to $iPOC_s$ with maximum values 5–6 g m^{-2} in early summer and minimum values <2.5 g m^{-2} in late winter both inside and outside the LBEZ (Figure 4b). Unlike $iPOC_s{}^{TZ}$, $iPOC_l{}^{TZ}$ peaked both inside and outside LBEZ around July. Except for September, there was on average ~30%

more total water-column $iPOC_l$ outside the LBEZ than inside. The vertical distribution of POC_l was fairly uniform, as $z^{50}{}_l$ was near 500 m for most of the year. For spring and summer, $z^{50}{}_l$ was ∼50 m shallower outside the LBEZ, indicating a higher proportion of POC_l nearer the surface. When comparing iPOC in small and large pools, $iPOC_l$ was lower than $iPOC_s$ by a factor of 2–4, with the bulk of this difference originating within the PZ and the lowest proportions of small-to-large POC during winter (Figure S13 in Supporting Information S1). Overall, total water-column iPOC was composed of a lower proportion of POC_l inside compared with outside the LBEZ (e.g., 36% of profiles have small-to-large POC >3 inside vs. 26% outside LBEZ; Figure S13c in Supporting Information S1), and iPOC was lower inside the LBEZ (annual iPOC sum 118 ± 17 g m^{-2} inside vs. 136 ± 10 g m^{-2} outside LBEZ).

3.3. Net POC Fluxes and Transfer Efficiency

Rates of change in iPOC describing net monthly accumulation or loss within various depth-zones are explored in Figures 4c–4f. Net accumulation of POC in the PZ began during January both inside and outside the LBEZ, peaking at ∼60 mg m^{-2} d^{-1} between March and May (Figures 4c and 4d). During spring, losses probably due to sinking and grazing began to counterbalance the increases in $iPOC^{PZ}$ until they outweighed primary production during July, at which point net losses prevailed in the PZ until January. Throughout spring and summer, losses inside the LBEZ productive zone were primarily due to small particles, as E_l^{PZ} was only 6%–13% of E^{PZ}, except for September where E_l^{PZ} was 50% of E^{PZ} (Figure S11 in Supporting Information S1). During 7 of 12 months, E^{PZ} was lower inside the LBEZ with a minimum in June of −66 ± 14 mg m^{-2} d^{-1} versus −45 ± 11 mg m^{-2} d^{-1} outside, suggesting higher losses within the PZ of the LBEZ. In the TZ, differences inside versus outside the LBEZ were more distinguishable and discussed in greater detail in Section 4.

4. Discussion

Overall, there was less iPOC *inside* the LBEZ compared to surrounding waters, and this is predominantly due to differences in the TZ (annual $iPOC^{TZ}$ sum 74 ± 15 g m^{-2} inside vs. 94 ± 8 g m^{-2} outside LBEZ). Here we unravel seasonal signatures to understand the mechanisms and drivers of this key difference.

Early spring – *Shoaling of deep mixed layers increases export inside the LBEZ.*

E^{TZ} in April was positive and nearly three times greater inside the LBEZ (Figures 4c and 4d), likely due to shoaling of deep winter mixed layers which can transport POC to depth (Dall'Olmo et al., 2016). High E^{TZ} driven by spring shoaling has been previously reported in this region (Dall'Olmo & Mork, 2014) and this mixed layer pump is more efficient inside the LBEZ (Figure 4e). A continued signature of the mixed layer pump may also be seen during May when MLDs are still largely varying inside the LBEZ (Figure 2b); however, much of E^{TZ} was accounted for in the upper-TZ as seen in the lower TE, especially to PZD^{+500}, inside the LBEZ (Figure 4e).

Late spring/early summer – *Increased production is countered by increased remineralization inside the LBEZ.*

While $iPOC_s^{PZ}$ was greater inside the LBEZ compared to surroundings during June–August, E^{PZ} was more negative inside the LBEZ suggesting greater losses, either due to remineralization or sinking. Considering E^{TZ} was also lower inside the LBEZ and E^{PZ} was predominately due to small particle losses (Figure S11 in Supporting Information S1), we believe this lower accumulation is more likely due to remineralization occurring in the PZ and upper-TZ. Enhanced AOU in the PZ and upper-TZ during late spring and early summer also indicates remineralization, as does lower TE (Figure 3l; Figure 4e) and increased nitrate concentrations (Figure S15 in Supporting Information S1) inside the LBEZ.

Late summer – *Large particles increase export inside the LBEZ.*

The only month with notably increased $iPOC_l^{TZ}$ inside the LBEZ compared with outside was September (Figure 3i; Figure 4b). This enhanced presence of large particles appears along with a brief period of positive E^{TZ} and high TE (Figures 4c and 4e). This positive E^{TZ} is primarily driven by an increase in POC_s inside the LBEZ—a potential signal of particle fragmentation (Briggs et al., 2020; Giering et al., 2014) perhaps driven by increased turbulence within the eddy (Fer et al., 2018; Zhu et al., 2023). The source of large particles may be aggregates or zooplankton fecal pellets considering the signature of higher AOU at the base of the PZ in September (Figure 3j). The observation may also be linked to eddy driven subduction (see also deepening 5°C isotherm in Figure 3a). Further evidence of particle fragmentation is also seen during July inside and outside LBEZ, where there is a

notable accumulation of POC_s in the lower TZ while there are net losses over the entire TZ when including POC_l (Figures 4c and 4d).

Summer/autumn – *A stronger biological carbon pump outside the LBEZ.*

Importantly, our findings for inside the LBEZ may be influenced by comparisons with a stronger biological carbon pump outside the LBEZ. Although it is not as apparent in TE, the sustained increase in POC_s outside the LBEZ at 600–1,000 m for June–December is indeed indicative of effective export out of the twilight zone (Figure 3e). This may be supported by faster sinking rates outside the LBEZ compared with inside during these months, as there were higher proportions of $iPOC_l^{TZ}$:$iPOC_s^{TZ}$ (Figure S13b in Supporting Information S1) and overall larger average particle diameters in the PZ (Figure S14 in Supporting Information S1). Alternatively, and perhaps additionally, remineralization may have been lower outside the LBEZ due to differences in microbial community composition considering observations of a higher $Chla_s$:b_{bps} and lower nitrate concentrations in the PZ outside the LBEZ during June–September (Figure S15 in Supporting Information S1).

Autumn – *Subduction drives high export and high efficiency inside the LBEZ.*

A relatively strong signature of subducting POC is evident inside the LBEZ from November to December: net accumulation in the TZ (Figure 4c) during November and increasing POC_s with increasing depth to ~200–600 m (Figures 2l and 3d) and on average 30% more POC at 400–800 m in December compared with outside the LBEZ (Figure 3f). Furthermore, the average 5°C isotherm deepens from 300 m in November to 440 m in December, marking the greatest deepening of this isotherm throughout the year (Figure 3a). It has also been suggested that the highest relative importance of the eddy subduction pump occurs during the autumn–winter period (Boyd et al., 2019).

Winter – *Enhanced remineralization in the hot tub of the Arctic.*

Although the late autumn subduction drives enhanced export of POC_s in the LBEZ, this material appears to return to the food web over winter. Greater losses were observed inside the LBEZ compared with outside during winter (Figures 4c and 4d). While more negative E^{TZ} could be from sinking or physical transport, we argue that remineralization was the main driver of these losses during winter considering large particles were at most ~30% of E^{TZ} inside the LBEZ (Figure 4c). During January–February, POC_s was ~30% *higher* at 500–800 m inside the LBEZ compared with outside, while it was ~45% *lower* below 800 m and TE also tends to be lower inside the LBEZ. It was ~1–4°C warmer inside the LBEZ's TZ during winter (Figure 3c), hence our designation of the LBEZ as the "hot tub of the Arctic." Increased temperature can enhance respiration and carbon demand leading to higher grazing rates of zooplankton and microbial activity (e.g., Boscolo-Galazzo et al., 2021; Lewandowska et al., 2014; Vázquez-Domínguez et al., 2007). Although AOU was not higher below ~200 m inside versus outside the LBEZ, we note a clear signature of increased AOU directly beneath the PZ of the LBEZ despite ventilation by deep winter mixed layers (Figure 3j).

5. Concluding Remarks

Observational studies on the biogeochemical roles of mesoscale eddies have been limited to episodic events, making it difficult to discern their seasonal behaviors and overall influence. The persistence of the LBE enabled us to harness over a decade of BGC-Argo data to build a monthly composite of its biogeochemical properties and study its influence on the biological carbon pump. We show that the LBEZ has distinctively warmer subsurface waters year-round and more production of POC contained in small particles in the near-surface during late spring and summer. Despite potential for year-round export driven by the eddy subduction pump within the LBEZ, a consistent increase in export and efficiency was not observed in the LBEZ. Although there is evidence of increased primary production and export inside the LBEZ during specific months, POC accumulation rates in the PZ and transfer efficiencies within the TZ were often lower compared to surrounding waters. Our analysis suggests higher respiration and slower particle sinking speeds combine to sustain increased remineralization of POC within the PZ of the LBEZ year-round, while warmer subsurface waters may support increased remineralization of subducted POC over winter.

In terms of broader biogeochemical roles of the LBEZ, the lower accumulation and vertical transfer efficiency of POC may be indicative of energy transfer higher up the food chain. Dong et al. (2022) traced a predominant supply of particles populating the Norwegian coast to the LBEZ using physical transport simulations; they

postulate that the LBEZ may be a spawning or overwintering location for the copepod *C. finmarchicus*, which crucially support fisheries in spring and summer. Other studies also found enhanced signatures of higher trophic level organisms within the twilight zone of Atlantic anticyclonic eddies (e.g., Della Penna & Gaube, 2020; Fennell & Rose, 2015; Gødo et al., 2012), and our study suggests the LBEZ is more conducive to the remineralization processes necessary to sustain higher trophic level organisms and effectively reduce organic carbon export by the biological carbon pump.

Data Availability Statement

BGC-Argo data were downloaded from the Coriolis Global Data Assembly Center on 2 May 2024 using the OneArgo Matlab toolbox (Frenzel et al., 2022). BGC-Argo data are freely available at Argo (2025). This study also relied on the freely available AVISO META3.2 DT allsat eddy atlas data to identify and track the LBE (Pegliasco, Busché, & Faugère, 2022). Global Ocean Colour Plankton MY L4 monthly observations from merged satellite data (ESA-CCI) was downloaded from Copernicus Marine Services on 26 December 2024 and data are freely available at https://doi.org/10.48670/moi-00283 (Global Ocean Colour Plankton MY L4 monthly observations, 2024). Data processing software and final processed data are freely available (Koestner, 2025).

Acknowledgments
This research was funded by the European Union under Marie Skłodowska-Curie Grant 101034309 to DK, and Grant 101083922 (OceanICU) to SC. The work was also supported by the UK Research and Innovation (UKRI) under the UK government's Horizon Europe funding guarantee (Grants 10054454, 10063673, 10064020, 10059241, 10079684, 10059012, 10048179) to SC. We would like to express our gratitude to the Norwegian Institute of Marine Research, and specifically to Kjell Arne Mork and Henrik Søiland for their tireless efforts in support of the NorArgo program and deployment of BGC-Argo floats in the Norwegian Sea. We also wish to acknowledge facilitators of the GO-BGC Float Data Workshop in 2023 where this study originated, including workshop group members Sawyer Brand, Prince Prakash, and Vic Dina. Additional thanks to Nathan Briggs for fruitful discussions regarding backscattering data processing and results, and to two anonymous reviewers for their valuable comments.

References

Argo. (2025). *Argo float data and metadata from Global Data Assembly Centre (Argo GDAC)*. SEANOE. https://doi.org/10.17882/42182

Boscolo-Galazzo, F., Crichton, K. A., Ridgwell, A., Mawbey, E. M., Wade, B. S., & Pearson, P. N. (2021). Temperature controls carbon cycling and biological evolution in the ocean twilight zone. *Science*, *371*(6534), 1148–1152. https://doi.org/10.1126/science.abb6643

Bosse, A., Fer, I., Lilly, J. M., & Søiland, H. (2019). Dynamical controls on the longevity of a non-linear vortex: The case of the Lofoten Basin Eddy. *Scientific Reports*, *9*(1), 13448. https://doi.org/10.1038/s41598-019-49599-8

Boyd, P. W., Claustre, H., Levy, M., Siegel, D. A., & Weber, T. (2019). Multi-faceted particle pumps drive carbon sequestration in the ocean. *Nature*, *568*(7752), 327–335. https://doi.org/10.1038/s41586-019-1098-2

Boyd, P. W., & Trull, T. W. (2007). Understanding the export of biogenic particles in oceanic waters: Is there consensus? *Progress in Oceanography*, *72*(4), 276–312. https://doi.org/10.1016/j.pocean.2006.10.007

Briggs, N., Dall'Olmo, G., & Claustre, H. (2020). Major role of particle fragmentation in regulating biological sequestration of CO2 by the oceans. *Science*, *367*(6479), 791–793. https://doi.org/10.1126/science.aay1790

Buesseler, K. O., Boyd, P. W., Black, E. E., & Siegel, D. A. (2020). Metrics that matter for assessing the ocean biological carbon pump. *Proceedings of the National Academy of Sciences*, *117*(18), 9679–9687. https://doi.org/10.1073/pnas.1918114117

Dall'Olmo, G., Dingle, J., Polimene, L., Brewin, R. J., & Claustre, H. (2016). Substantial energy input to the mesopelagic ecosystem from the seasonal mixed-layer pump. *Nature Geoscience*, *9*(11), 820–823. https://doi.org/10.1038/ngeo2818

Dall'Olmo, G., & Mork, K. A. (2014). Carbon export by small particles in the Norwegian Sea. *Geophysical Research Letters*, *41*(8), 2921–2927. https://doi.org/10.1002/2014GL059244

Della Penna, A., & Gaube, P. (2020). Mesoscale eddies structure mesopelagic communities. *Frontiers in Marine Science*, *7*, 454. https://doi.org/10.3389/fmars.2020.00454

Dong, H., Zhou, M., Smith, W. O., Li, B., Hu, Z., Basedow, S. L., et al. (2022). Dynamical controls of the eastward transport of overwintering Calanus finmarchicus from the Lofoten Basin to the continental slope. *Journal of Geophysical Research: Oceans*, *127*(9), e2022JC018909. https://doi.org/10.1029/2022JC018909

Fennell, S., & Rose, G. (2015). Oceanographic influences on deep scattering layers across the North Atlantic. *Deep Sea Research Part I: Oceanographic Research Papers*, *105*, 132–141. https://doi.org/10.1016/j.dsr.2015.09.002

Fer, I., Bosse, A., Ferron, B., & Bouruet-Aubertot, P. (2018). The dissipation of kinetic energy in the Lofoten Basin Eddy. *Journal of Physical Oceanography*, *48*(6), 1299–1316. https://doi.org/10.1175/JPO-D-17-0244.1

Frenzel, H., Sharp, J., Fassbender, A., & Buzby, N. (2022). OneArgo-Mat: A MATLAB toolbox for accessing and visualizing Argo data (v1.0.3) [Software]. *Zenodo*. https://doi.org/10.5281/zenodo.7055484

Giering, S. L., Sanders, R., Lampitt, R. S., Anderson, T. R., Tamburini, C., Boutrif, M., et al. (2014). Reconciliation of the carbon budget in the ocean's twilight zone. *Nature*, *507*(7493), 480–483. https://doi.org/10.1038/nature13123

Global Ocean Colour Plankton MY L4 monthly observations. (2024). E.U. Copernicus Marine Service Information (CMEMS) [Dataset]. *Marine Data Store (MDS)*. https://doi.org/10.48670/moi-00283

Godø, O. R., Samuelsen, A., Macaulay, G. J., Patel, R., Hjøllo, S. S., Horne, J., et al. (2012). Mesoscale eddies are oases for higher trophic marine life. *PLoS One*, *7*(1), e30161. https://doi.org/10.1371/journal.pone.0030161

Helland-Hansen, B., & Nansen, F. (1909). The Norwegian Sea. Its physical oceanography based upon the Norwegian researches 1900 – 1904. Report on Norwegian Fishery and Marine Investigations, Vol. II, Part I. Fiskeridirektoratets, Bergen.

Honjo, S., Eglinton, T. I., Taylor, C. D., Ulmer, K. M., Sievert, S. M., Bracher, A., et al. (2014). Understanding the role of the biological pump in the global carbon cycle: An imperative for ocean science. *Oceanography*, *27*(3), 10–16. https://doi.org/10.5670/oceanog.2014.78

Isachsen, P. E., Koszalka, I., & LaCasce, J. H. (2012). Observed and modeled surface eddy heat fluxes in the eastern Nordic Seas. *Journal of Geophysical Research*, *117*(C8). https://doi.org/10.1029/2012JC007935

Ito, T., Follows, M. J., & Boyle, E. A. (2004). Is AOU a good measure of respiration in the oceans? *Geophysical Research Letters*, *31*(17). https://doi.org/10.1029/2004GL020900

Johnson, K. S., Riser, S. C., & Karl, D. M. (2010). Nitrate supply from deep to near-surface waters of the North Pacific subtropical gyre. *Nature*, *465*(7301), 1062–1065. https://doi.org/10.1038/nature09170

Koestner, D. (2025). DanielKoestner/LBE_BGC_GRL_Software: v1 (version v1) [Software]. *Zenodo*. https://doi.org/10.5281/zenodo.14850376

Koestner, D., Stramski, D., & Reynolds, R. A. (2024). Improved multivariable algorithms for estimating oceanic particulate organic carbon concentration from optical backscattering and chlorophyll-a measurements. *Frontiers in Marine Science*, *10*, 1197953. https://doi.org/10.3389/fmars.2023.1197953

Köhl, A. (2007). Generation and stability of a quasi-permanent vortex in the Lofoten Basin. *Journal of Physical Oceanography*, *37*(11), 2637–2651. https://doi.org/10.1175/2007JPO3694.1

Lacour, L., Llort, J., Briggs, N., Strutton, P. G., & Boyd, P. W. (2023). Seasonality of downward carbon export in the Pacific Southern Ocean revealed by multi-year robotic observations. *Nature Communications*, *14*(1), 1278. https://doi.org/10.1038/s41467-023-36954-7

Lévy, M., Couespel, D., Haëck, C., Keerthi, M. G., Mangolte, I., & Prend, C. J. (2024). The impact of fine-scale currents on biogeochemical cycles in a changing ocean. *Annual Review of Marine Science*, *16*(1), 191–215. https://doi.org/10.1146/annurev-marine-020723-020531

Lewandowska, A. M., Boyce, D. G., Hofmann, M., Matthiessen, B., Sommer, U., & Worm, B. (2014). Effects of sea surface warming on marine plankton. *Ecology Letters*, *17*(5), 614–623. https://doi.org/10.1111/ele.12265

Mason, E., Pascual, A., & McWilliams, J. C. (2014). A new sea surface height–based code for oceanic mesoscale eddy tracking. *Journal of Atmospheric and Oceanic Technology*, *31*(5), 1181–1188. https://doi.org/10.1175/JTECH-D-14-00019.1

McGillicuddy Jr, D. J. (2016). Mechanisms of physical-biological-biogeochemical interaction at the oceanic mesoscale. *Annual Review of Marine Science*, *8*(1), 125–159. https://doi.org/10.1146/annurev-marine-010814-015606

Omand, M. M., D'Asaro, E. A., Lee, C. M., Perry, M. J., Briggs, N., Cetinić, I., & Mahadevan, A. (2015). Eddy-driven subduction exports particulate organic carbon from the spring bloom. *Science*, *348*(6231), 222–225. https://doi.org/10.1126/science.1260062

Pegliasco, C., Busché, C., & Faugère, Y. (2022). Mesoscale eddy trajectory atlas META3.2 delayed-time all satellites (3.2 DT allsat 1993-01-01/2021-08-02) [Dataset]. *CNES*. https://doi.org/10.24400/527896/A01-2022.005

Pegliasco, C., Delepoulle, A., Mason, E., Morrow, R., Faugère, Y., & Dibarboure, G. (2022). META3. 1exp: A new global mesoscale eddy trajectory atlas derived from altimetry. *Earth System Science Data*, *14*(3), 1087–1107. https://doi.org/10.5194/essd-14-1087-2022

Raj, R. P., Johannessen, J. A., Eldevik, T., Nilsen, J. Ø., & Halo, I. (2016). Quantifying mesoscale eddies in the Lofoten Basin. *Journal of Geophysical Research: Oceans*, *121*(7), 4503–4521. https://doi.org/10.1002/2016JC011637

Rau, M. J., Ackleson, S. G., & Smith, G. B. (2018). Effects of turbulent aggregation on clay floc breakup and implications for the oceanic environment. *PLoS One*, *13*(12), e0207809. https://doi.org/10.1371/journal.pone.0207809

Resplandy, L., Lévy, M., & McGillicuddy Jr, D. J. (2019). Effects of eddy-driven subduction on ocean biological carbon pump. *Global Biogeochemical Cycles*, *33*(8), 1071–1084. https://doi.org/10.1029/2018GB006125

Rossby, T., Prater, M. D., & Søiland, H. (2009). Pathways of inflow and dispersion of warm waters in the Nordic seas. *Journal of Geophysical Research*, *114*(C4). https://doi.org/10.1029/2008JC005073

Søiland, H., Chafik, L., & Rossby, T. (2016). On the long-term stability of the Lofoten Basin Eddy. *Journal of Geophysical Research: Oceans*, *121*(7), 4438–4449. https://doi.org/10.1002/2016JC011726

Søiland, H., & Rossby, T. (2013). On the structure of the Lofoten Basin Eddy. *Journal of Geophysical Research: Oceans*, *118*(9), 4201–4212. https://doi.org/10.1002/jgrc.20301

Song, Y., Burd, A. B., & Rau, M. J. (2023). The deformation of marine snow enables its disaggregation in simulated oceanic shear. *Frontiers in Marine Science*, *10*, 1224518. https://doi.org/10.3389/fmars.2023.1224518

Stukel, M. R., Aluwihare, L. I., Barbeau, K. A., Chekalyuk, A. M., Goericke, R., Miller, A. J., et al. (2017). Mesoscale ocean fronts enhance carbon export due to gravitational sinking and subduction. *Proceedings of the National Academy of Sciences*, *114*(6), 1252–1257. https://doi.org/10.1073/pnas.1609435114

Vázquez-Domínguez, E., Vaque, D., & Gasol, J. M. (2007). Ocean warming enhances respiration and carbon demand of coastal microbial plankton. *Global Change Biology*, *13*(7), 1327–1334. https://doi.org/10.1111/j.1365-2486.2007.01377.x

Volk, T., & Hoffert, M. I. (1985). Ocean carbon pumps: Analysis of relative strengths and efficiencies in ocean-driven atmospheric CO2 changes. *The carbon cycle and atmospheric CO2: Natural variations Archean to present*, *32*, 99–110. https://doi.org/10.1029/GM032p0099

Wang, Y., Yang, J., & Chen, G. (2023). Euphotic zone depth anomaly in global mesoscale eddies by multi-mission fusion data. *Remote Sensing*, *15*(4), 1062. https://doi.org/10.3390/rs15041062

Zhu, X. Y., Yang, Z., Xie, Y., Zhou, K., & Wang, W. L. (2023). Strong particle dynamics counteract the nutrient-pumping effect leading to weak carbon flux in a cyclonic eddy. *Marine Chemistry*, *255*, 104279. https://doi.org/10.1016/j.marchem.2023.104279

References From the Supporting Information

Bittig, H. C., Maurer, T. L., Plant, J. N., Schmechtig, C., Wong, A. P., Claustre, H., et al. (2019). A BGC-Argo guide: Planning, deployment, data handling and usage. *Frontiers in Marine Science*, *6*, 502. https://doi.org/10.3389/fmars.2019.00502

Briggs, N. T., Slade, W. H., Boss, E., & Perry, M. J. (2013). Method for estimating mean particle size from high-frequency fluctuations in beam attenuation or scattering measurements. *Applied Optics*, *52*(27), 6710–6725. https://doi.org/10.1364/AO.52.006710

Dall'Olmo, G., Tvs, U. B., Bittig, H., Boss, E., Brewster, J., Claustre, H., & Xing, X. (2022). Real-time quality control of optical backscattering data from Biogeochemical-Argo floats. *Open Research Europe*, *2*. https://doi.org/10.12688/openreseurope.15047.2

de Boyer Montégut, C., Madec, G., Fischer, A. S., Lazar, A., & Iudicone, D. (2004). Mixed layer depth over the global ocean: An examination of profile data and a profile-based climatology. *Journal of Geophysical Research*, *109*(C12). https://doi.org/10.1029/2004JC002378

Owens, S. A., Pike, S., & Buesseler, K. O. (2015). Thorium-234 as a tracer of particle dynamics and upper ocean export in the Atlantic Ocean. *Deep Sea Research Part II: Topical Studies in Oceanography*, *116*, 42–59. https://doi.org/10.1016/j.dsr2.2014.11.010

Poteau, A., Boss, E., & Claustre, H. (2017). Particulate concentration and seasonal dynamics in the mesopelagic ocean based on the backscattering coefficient measured with Biogeochemical-Argo floats. *Geophysical Research Letters*, *44*(13), 6933–6939. https://doi.org/10.1002/2017GL073949

Roesler, C., Uitz, J., Claustre, H., Boss, E., Xing, X., Organelli, E., et al. (2017). Recommendations for obtaining unbiased chlorophyll estimates from in situ chlorophyll fluorometers: A global analysis of WET Labs ECO sensors. *Limnology and Oceanography: Methods*, *15*(6), 572–585. https://doi.org/10.1002/lom3.10185

Serra-Pompei, C., & Dutkiewicz, S. (2024). Phytoplankton Chlorophyll trends in the Arctic at the local, regional, and pan-Arctic scales (1998–2022). *Geophysical Research Letters*, *51*(23), e2024GL110454. https://doi.org/10.1029/2024GL110454